MULTISCALE ANALYSIS FOR DYNAMIC CONTACT ANGLE HYSTERESIS ON ROUGH SURFACES*

SI XIAO †, XIANMIN XU ‡, AND ZHEN ZHANG §

Abstract. Dynamic contact angle hysteresis is of critical importance for many two-phase flow problems with moving contact lines. It is induced by inhomogeneity or roughness of the substrates. In this paper, we present theoretical studies on the time averaging of a reduced model for wetting on rough surfaces and also the analysis on the effect of stochastic thermal forces. We derive equations for the averaged dynamics and show that the apparent contact angle depends on the harmonic averaging of the geometric and chemical properties of the substrates as well as the contact line velocity. The contact angle hysteresis can be determined quantitatively by the equations. The averaging results are proved rigorously by multi-scale analysis and verified by some numerical examples.

1. Introduction. Wetting on rough surfaces has many applications in industry and our daily life. It has attracted much interest in many different fields [8, 22, 4, 10]. If without considering the dynamics of fluids, wetting is a problem to minimize the total surface energy in the system. Mathematically, wetting on rough surface gives a free interface problem with multi-scale boundary conditions and has been studied a lot recently, see for example in [1, 5, 2, 19, 35, 6, 33, 11, 32]. Various numerical methods have also been developed for wetting problems based on different models models [30, 18, 12, 13].

Dynamic wetting is a typical two-phase flow with moving contact lines. The standard no slip boundary conditions for viscous fluids will lead to infinite energy dissipation when the contact line moves. There are extensive studies on the moving contact line problem [7, 21, 3, 24, 26, 29], while there still exist some controversies [27]. If one further consider the effect of the rough surfaces, the problem will be much more complicated [17, 23, 14, 31, 25]. In general the advancing and receding contact angles will be different and may depend on the contact line velocity. Such phenomena are called contact angle hysteresis(CAH). It is of critical importance to quantitatively study the wetting phenomena in many applications.

In [39], a macroscopic boundary condition is derived for the dynamic contact angle hysteresis on chemically inhomogeneous surfaces, which has been used to explain the dynamic contact angle hysteresis recently observed in experiments [15, 16]. The key idea there is to use the Onsager variational principle [9] and asymptotic analysis to derive a coarse graining boundary condition for the apparent contact angle. The boundary condition gives results fit with experiments very well [36, 39]. The boundary conditions can also be coupled with the standard two-phase Navier-Stokes equation to simulate two-phase flows with moving contact lines[38].

The main contributions of the paper are three folds. Firstly, we generalize the analysis in [39] to wetting on surfaces with both geometrical roughness and chemical

*This work is partially supported by NSFC grant (No. 11971469) and by the National Key R&D Program of China under Grant 2018YFB0704304 and Grant 2018YFB0704300.

†LSEC, ICMSEC, NCMIS, Academy of Mathematics and Systems Science, Chinese Academy of Sciences, Beijing 100190, China; University of Chinese Academy of Sciences, Beijing 100049, China, xiaosi@lsec.cc.ac.cn

‡ LSEC, ICMSEC, NCMIS, Academy of Mathematics and Systems Science, Chinese Academy of Sciences, Beijing 100190, China; Corresponding author, xmxu@lsec.cc.ac.cn.

§Department of Mathematics, International Center for Mathematics, National Center for Applied Mathematics (Shenzhen),Guangdong Provincial Key Laboratory of Computational Science and Material Design, Southern University of Science and Technology (SUSTech), Shenzhen 518055, P.R. China.zhangz@sustech.edu.cn

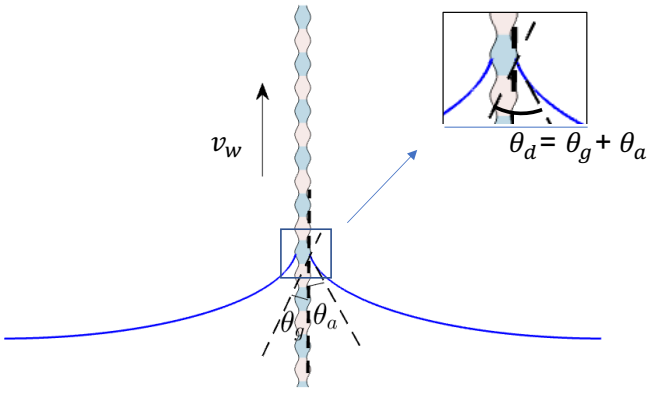

FIG. 1. *The fiber with smooth oscillating boundaries*

inhomogeneity. We derive an equation for the time averaged system when the roughness coefficient goes to zero. It leads to an explicit formula for the dynamic contact angle hysteresis on such surfaces. This will be much more useful in many applications than that only considering chemical inhomogeneity of the substrates. Secondly, we characterize quantitatively the effect of stochastic thermal forces by a detailed analysis for a stochastic model. We study the time averaging for the stochastic model and derive an averaged system by asymptotic analysis for the backward Kolmogrov equation. We derive a new formula for the contact angle hysteresis, which takes account of the stochastic effects. We also show that the averaged system converges to that of the deterministic model when the stochastic coefficient goes to zero. Thirdly, we present rigorous analysis for the asymptotic results, which has not been studied even for the simple problem with chemically inhomogeneous surfaces before.

The rest of the paper is organized as follows. In section 2, we derive some reduced models for dynamic wetting problems. In section 3, we present the analysis for the deterministic model. We derive an averaged system and prove that the original system converges to the averaged one when the period of the oscillations goes to zero. In section 4, we study the averaging of a stochastic system which describes the effect of the stochastic thermal forces. Several numerical examples are illustrated in Section 5 to verify our theoretical results. Some concluding remarks are given in the last section.

2. Reduced models for dynamic wetting. We develop a reduced model for some dynamic wetting problems in this section. We first introduce two illustrative examples and then show a general model in the last subsection.

2.1. Forced wetting of a fiber. We consider the motion of a fiber in a liquid reservoir, as shown in Figure 1. This is motivated by the recent experiments in [15]. Suppose that the surface of the fiber is rough and inhomogeneous. For simplicity, we assume that the surface is axis-symmetric and the radius of the section is described by a function

$$r = R(z) = R_0 + \varepsilon R_1(\frac{z}{\varepsilon})$$

where R_0 is a positive constant and $R_1(\cdot)$ is a smooth function with periodic 1, and $\varepsilon \ll 1$ is a small parameter. The wetting property of the solid surface is characterized by the Young's angle $\theta_Y(\frac{z}{\varepsilon})$, which is a function of z with a period ε. When the fiber moves with a velocity v_w, the solid surface at time t is given by

$$r = \tilde{R}(z,t) := R_0 + \varepsilon R_1(\frac{z - v_w t}{\varepsilon}). \tag{1}$$

For a liquid-vapor interface on the rough surface, the local contact angle θ_d is the angle between the tangential plane of the interface and that of the solid surface on the contact line. It is usually different from the apparent contact angle θ_a, which is the angle between the two-phase interface and the the homogenized surface of the substrate(the vertical surface in this example). As shown in Figure 1, we have

$$\theta_d = \theta_a + \theta_g, \tag{2}$$

where θ_g characterizes the local slope of the oscillating substrate on the contact line and is given by $\theta_g = \arctan\left(R_1'(\frac{z_{ct} - v_w t}{\varepsilon})\right)$. Here we denote by z_{ct} the vertical coordinate of the contact line.

In equilibrium states, the local contact angle θ_d is equal to the local Young's angle. However, when the interface is moving, the contact angle θ_d can be different from θ_Y. By using the Onsager principle as an approximation tool, we derive an equation for the dynamic contact angle in [39],

$$\frac{\mu v_{ct}}{\mathcal{F}(\theta_d)} = \gamma(\cos\theta_Y - \cos\theta_d), \tag{3}$$

where μ is the viscosity of the liquid, γ is the surface tension of the interface, and $\mathcal{F}(\theta_d) = \left(\alpha + \frac{2|\ln\zeta|\sin^2\theta_d}{\theta_d - \sin\theta_d\cos\theta_d}\right)^{-1}$, α is a friction parameter of the contact line, and ζ is a dimensionless cut-off parameter. The equation shows that the unbalanced Young force is equal to the viscous friction force near the contact line. It is the first order approximation of the well-known Cox's formula (c.f. [7]) when the capillary number $Ca = \mu v/\gamma$ is small.

As shown in [15], when the fiber is thin, the liquid surface approaches very rapidly to its equilibrium shape, which is given by [8, 34]

$$z = H(r) = h(t) - \tilde{R}(z_{ct},t)\cos\theta_a \ln\frac{r + \sqrt{r^2 - \tilde{R}^2(z_{ct},t)\cos^2\theta_a}}{\tilde{R}(z_{ct},t)\cos\theta_a}. \tag{4}$$

This indicates a geometrical relation between the contact line position z_{ct} and the apparent contact angle θ_a.

By the equations (3) and (4) and by setting $\hat{z}_{ct} = z_{ct} - v_w t$, we can derive an ordinary differential system as follows (see details in Appendix A),

$$\begin{cases} \dot{\hat{z}}_{ct} = f(\theta_a, \hat{z}_{ct})(\cos\theta_Y(\hat{z}_{ct}) - \cos(\theta_a + \theta_g(\hat{z}_{ct}))), \\ \dot{\theta}_a = -g_1(\theta_a, \hat{z}_{ct})\Big(g_2(\theta_a, \hat{z}_{ct})\dot{\hat{z}}_{ct} + v_w\Big), \end{cases} \tag{5}$$

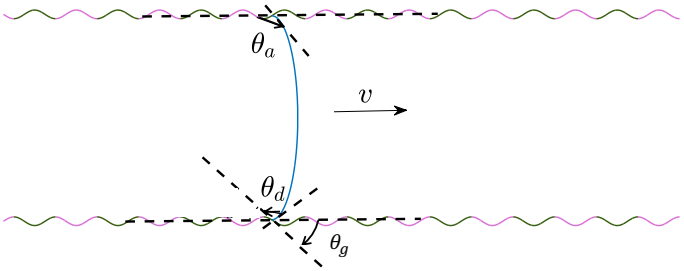

FIG. 2. *The channel with smooth oscillating boundaries*

where

$$f(\theta_a,\hat{z}_{ct}) = \frac{\gamma\mathcal{F}(\theta_d)\cos\theta_g}{\mu} = \frac{\gamma}{\mu}\left(\alpha + \frac{2|\ln\zeta|\sin^2\theta_d}{\theta_d - \sin\theta_d\cos\theta_d}\right)^{-1}\left(1+\left(R_1'(\frac{\hat{z}_{ct}}{\varepsilon})\right)^2\right)^{-\frac{1}{2}},$$
$$g_1(\theta_a,\hat{z}_{ct}) = \frac{1}{\left(R_0+\varepsilon R_1(\frac{\hat{z}_{ct}}{\varepsilon})\right)\left(\sin\theta_a\mathscr{G}(\theta_a,\hat{z}_{ct})+1\right)},$$
$$g_2(\theta_a,\hat{z}_{ct}) = 1 - R_1'(\frac{\hat{z}_{ct}}{\varepsilon})\mathscr{G}(\theta_a,\hat{z}_{ct})\cos\theta_a,$$

with $\mathscr{G}(\theta_a,\hat{z}_{ct}) \approx \ln\frac{2r_c}{R(\hat{z}_{ct})(1+\sin\theta_a)} - 1$. Equ. (5) is a reduced model for the forced wetting problem of a moving fiber. When the surface is flat, (5) is reduced to a model for chemically inhomogeneous surfaces in [34, 39].

2.2. Dynamict wetting in a capillary tube. In the second example, we consider the imbibition of a liquid in a two-dimensional channel with oscillating and inhomogeneous boundaries. As shown in Figure 2, suppose that the boundaries of the channel are given by $z = \pm(h_0 + \varepsilon h_1(\frac{x}{\varepsilon}))$, where h_0 is a positive number, $h_1(\cdot)$ is a smooth function with periodic 1 and $\varepsilon \ll 1$ is a small parameter. The chemical inhomogeneity of the boundaries is characterized by the Young's angle $\theta_Y(\frac{x}{\varepsilon})$ which is a periodic function with period ε. Similarly as in the above example, $\theta_d = \theta_a + \theta_g$ gives a relation between the local contact angle θ_d, the apparent contact angle θ_a, and an angle $\theta_g = \arctan h_1'(\frac{x_{ct}}{\varepsilon})$ characterizing the local slope of the oscillating substrates.

Suppose the two-phase interface moves to the right with a velocity v. The relation between the local dynamic contact angle θ_d and the contact line velocity is still given by (3). When the height of the channel is very small, we can assume that the shape of the interface is circular. This leads to an additional constraint on the contact point position and the apparent contact angle θ_a. Similar to the derivation in previous example (c.f. [37]), we can derive a system of ordinary differential equations as follows,

$$\text{(6)}\qquad \begin{cases} \dot{x}_{ct} = \tilde{f}(\theta_a,x_{ct})(\cos\theta_Y(\frac{x_{ct}}{\varepsilon}) - \cos\theta_d), \\ \dot{\theta}_a = -\tilde{g}_1(\theta_a,x_{ct})\Big(\tilde{g}_2(\theta_a,x_{ct})\tilde{f}(\theta_a,x_{ct})(\cos\theta_Y(\frac{x_{ct}}{\varepsilon}) - \cos\theta_d) - \frac{h_0}{h(x_{ct})}v\Big), \end{cases}$$

where

$$\tilde{f}(\theta_a, x_{ct}) = \frac{\gamma}{\mu}\left(\alpha + \frac{2|\ln\zeta|\sin^2\theta_d}{\theta_d - \sin\theta_d\cos\theta_d}\right)^{-1}\left(1 + \left(h_1'(\frac{x_{ct}}{\varepsilon})\right)^2\right)^{-\frac{1}{2}},$$
$$\tilde{g}_1(\theta_a, x_{ct}) = \frac{\cos\theta_a^3}{h(x_{ct})(\cos\theta_a + (\theta_a - \frac{\pi}{2})\sin\theta_a)},$$
$$\tilde{g}_2(\theta_a, x_{ct}) = 1 + h_1'(\frac{x_{ct}}{\varepsilon})\frac{\theta_a - \frac{\pi}{2} + \sin\theta_a\cos\theta_a}{\cos^2\theta_a}.$$

with $h(x_{ct}) = h_0 + \varepsilon h_1(\frac{x_{ct}}{\varepsilon})$. Equ. (6) is a reduced model for imbibition in a microchannel. It is easy to see that Equ. (6) has the same structure with (5). Furthermore, the viscous dissipation coefficient $\tilde{f}(\cdot,\cdot)$ has the same form as $f(\cdot,\cdot)$.

2.3. A general reduced model for dynamic wetting. The previous examples motivate us to consider a general mathematical model for dynamic wetting on rough and inhomogeneous solid surfaces. It is a system of ordinary differential equations for the contact point x_{ct} and the apparent contact angle θ_a:

$$\dot{x}_{ct} = f(\theta_a, \frac{x_{ct}}{\varepsilon})\Big(\cos\theta_Y(\frac{x_{ct}}{\varepsilon}) - \cos(\theta_a + \theta_g(\frac{x_{ct}}{\varepsilon}))\Big) + \varepsilon r_1(\theta_a, \frac{x_{ct}}{\varepsilon}, v) \tag{7a}$$
$$\dot{\theta}_a = -g(\theta_a)\Big((1 + p(\theta_a, \frac{x_{ct}}{\varepsilon}))\dot{x}_{ct} - v\Big) + \varepsilon r_2(\theta_a, \frac{x_{ct}}{\varepsilon}, v). \tag{7b}$$

Here v denotes the fluid velocity and $\varepsilon > 0$ is a small roughness parameter. The Young's angle $\theta_Y(\cdot)$ and the geometric angle $\theta_g(\cdot)$ respectively characterize the chemical and geometrical roughness of the substrate. $f(\cdot)$ characterizes the viscous dissipation coefficient near the contact line, which depends only on the physical property of the fluid and the local oscillations of the substrate. g and p are functions depends on the specific setups of the problem. εr_1 and εr_2 represent two possible higher order terms. We make the following assumptions on the functions in the system:

- (**A1**). All the functions $f(\theta, y), g(\theta), p(\theta, y), r_1(\theta, v, y), r_2(\theta, v, y), \theta_Y(y), \theta_g(y)$ are smooth functions and periodic in y with period 1. Furthermore, we have $\int_0^1 p(\theta, y)dy = 0$.
- (**A2**). There exists a positive constant c_0 such that $f, g, p \geq c_0 > 0$.
- (**A3**). There exists two constants $\theta_1, \theta_2 \in (0, \pi)$ such that

$$0 < \theta_1 \leq \theta_Y(y) - \theta_g(y) \leq \theta_2 < \pi, \qquad \forall y \in (0, 1].$$

The general model (7) covers the equations (5) and (6) in previous subsections. For example, $g(\theta)$ can be seen as the leading order term of the Taylor expansion of g_1 in (5) with respect to ε and the higher order terms are included in εr_2. In addition, it also covers a model in [37] which is derived from the sharp-interface limit of the phase-field equation.

In some cases, there may exist stochastic forces (e.g. thermal force) that affect the motion of contact lines [15, 16]. We add a stochastic force term in (7) and obtain a stochastic differential equation,

$$\dot{x}_{ct} = f(\theta_a, \frac{x_{ct}}{\varepsilon})(\cos\theta_Y(\frac{x_{ct}}{\varepsilon}) - \cos(\theta_a + \theta_g(\frac{x_{ct}}{\varepsilon})) + \sigma\sqrt{\varepsilon}\dot{W}) + \varepsilon r_1\Big(\theta_a, \frac{x_{ct}}{\varepsilon}, v\Big), \tag{8a}$$
$$\dot{\theta}_a = -g(\theta_a)\Big((1 + p(\theta_a, \frac{x_{ct}}{\varepsilon}))\dot{x}_{ct} - v\Big) + \varepsilon r_2\Big(\theta_a, \frac{x_{ct}}{\varepsilon}, v)\Big), \tag{8b}$$

where $W(t)$ is a Brownian motion and σ is a constant coefficient. Here we assume that the stochastic force is relatively small so that there is a factor $\sqrt{\varepsilon}$ in the coefficient.

3. Time averaging of the deterministic model. We are interested in the averaged dynamics of the systems (7) and (8) when ε goes to zero. For simplicity in presentation, we introduce a fast variable $y_{ct} = \frac{x_{ct}}{\varepsilon}$ and some notations. The system (7) can be transformed to:

$$\dot{y}_{ct} = \frac{1}{\varepsilon} A(\theta_a, y_{ct}) + F_1(\theta_a, y_{ct}, v), \tag{9a}$$

$$\dot{\theta}_a = B(\theta_a, y_{ct}) + \varepsilon F_2(\theta_a, y_{ct}, v), \tag{9b}$$

where

$$\begin{aligned} A(\theta, y) &= f(\theta, y)(\cos\theta_Y(y) - \cos(\theta + \theta_g(y))), \\ B(\theta, y) &= -g(\theta)\Big((1 + p(\theta, y))A(\theta, y) - v\Big) \\ F_1(\theta, y) &= r_1(\theta, y, v) \\ F_2(\theta, y, t) &= -g(\theta)(1 + p(\theta, y))r_1(\theta, y, v) + r_2(\theta, y, v). \end{aligned}$$

In this section, we first derive the averaged equation of (9) by asymptotic analysis and then prove the results rigorously.

3.1. The case with an invariant manifold. It turns out that the averaging of Equ. (9) depends on the range of the apparent contact angle θ_a. In this subsection, we show that there may exist an invariant manifold for the dynamic system when θ_a is in an interval $(\theta_1 + O(\varepsilon), \theta_2 + O(\varepsilon))$.

Since $A(\theta, y) = f(\theta, y)(\cos\theta_Y(y) - \cos(\theta + \theta_g(y)))$ and $f > 0$, we know that $A(\theta, y) = 0$ only when $\theta_Y(y) = \theta + \theta_g(y)$. By Assumption (A3), this happens when $\theta \in [\theta_1, \theta_2]$. Notice both $A(\theta, \cdot)$ and $F_1(\theta, \cdot, v)$ are smooth and periodic functions for any fixed θ and v. There exists an interval $(\theta_1 + O(\varepsilon), \theta_2 + O(\varepsilon))$, such that any θ in the interval corresponds to a value $y = \Psi(\theta)$ satisfying $A(\theta, \Psi(\theta)) + \varepsilon F_1(\theta, \Psi(\theta), v) = 0$ and $\partial_y A(\theta, \Psi(\theta)) + \varepsilon \partial_y F_1(\theta, \Psi(\theta), v) \leq 0$. The graph $(\theta, \Psi(\theta))$ is called *an invariant manifold* of (9) (see definition in [20]), since (θ_a, y_{ct}) will move along the graph except a possible intial layer when $\theta_a \in (\theta_1 + O(\varepsilon), \theta_2 + O(\varepsilon))$. (This can be easily seen from Equ. (9a).)

Hereinafter, we denote by

$$\Gamma = \{(\theta, y) | y = \Psi(\theta)\},$$

the invariant manifold of (9). Then we easily derive

$$\frac{\mathrm{d}y}{\mathrm{d}t}\Big|_\Gamma = \partial_\theta \Psi(\theta) \frac{\mathrm{d}\theta}{\mathrm{d}t}.$$

Equ. (9) is reduced to

$$\partial_\theta \Psi(\theta_a) \frac{\mathrm{d}\theta_a}{\mathrm{d}t} = \frac{1}{\varepsilon} A(\theta_a, \Psi(\theta_a)) + F_1(\theta_a, \Psi(\theta_a), v) \tag{10a}$$

$$\frac{d\theta_a}{dt} = B(\theta_a, \Psi(\theta_a)) + \varepsilon F_2(\theta_a, \Psi(\theta_a), v). \tag{10b}$$

This leads to

$$\partial_\theta \Psi(\theta_a)(B(\theta_a, \Psi(\theta_a)) + \varepsilon F_2(\theta_a, \Psi(\theta_a), v)) = \frac{1}{\varepsilon} A(\theta_a, \Psi(\theta_a)) + F_1(\theta_a, \Psi(\theta_a), v) \tag{11}$$

Suppose that the function $\Psi(\theta)$ has the following formal expansion:

$$\Psi(\theta) = \Psi_0(\theta) + \varepsilon\Psi_1(\theta) + \mathcal{O}(\varepsilon^2).$$

We substitute the expansion into (11). In leading order of ε, we have

$$\mathcal{O}(\varepsilon^{-1}): \qquad A(\theta_a, \Psi_0(\theta_a)) = 0.$$

By the formula of A, the equation has a solution only when $\theta_a \in [\theta_1, \theta_2]$. Notice that $A(\theta, \cdot)$ is a periodic function with period 1. We can assume that $\Psi_0(\theta) = k + \eta(\theta)$ with $k \in \mathbb{Z}$ and $\eta(\theta) \in (0, 1]$ satisfying $A(\theta, \eta(\theta)) = 0$ and $\partial_y A(\theta, \eta(\theta)) \le 0$. Then the leading order of Equ. (10b) is reduced to

$$\mathcal{O}(1): \qquad \frac{d\theta_a}{dt} = B(\theta_a, \Psi_0(\theta_a)) = g(\theta_a)v.$$

where we use the formula of B.

In summary, for a small ε, the leading order approximation of (9) when $\theta_a \in [\theta_1, \theta_2]$ is given by

$$\frac{\mathrm{d}\Theta}{\mathrm{d}t} = vg(\Theta), \quad y_{ct}^{(0)} = k + \eta(\Theta), \tag{12}$$

where $\eta(\theta)$ satisfies

$$A(\theta, \eta(\theta)) = 0, \quad \partial_y A(\theta, \eta(\theta)) \le 0, \quad \eta(\theta) \in [0, 1),$$

and the integer k depends on the initial condition of y_{ct}.

3.2. The general case. By Equ. (12), we see that θ will increase monotonously when $v > 0$ (or decrease monotonously when $v < 0$) noticing that $g(\cdot) \ge c_0 > 0$ in Assumption (A2). Therefore, even when $\theta \in [\theta_1, \theta_2]$ initially, it will go out of the interval soon. In this subsection, we derive the leading order approximation for (9) in the general case when $\theta \notin [\theta_1, \theta_2]$, by considering the formal approximation expansion of the backward Kolmorov equation of (9) (c.f. [20]).

The backward Kolmorov equation of Equ. (9) is a partial differential equation

$$\frac{\partial \phi}{\partial t} = \mathcal{L}\phi, \tag{13}$$

with the generator $\mathcal{L} = \frac{1}{\varepsilon}\mathcal{L}_0 + \mathcal{L}_1 + \varepsilon\mathcal{L}_2$ and

$$\begin{aligned} \mathcal{L}_0 &= A(\theta, y)\partial_y, \\ \mathcal{L}_1 &= B(\theta, y)\partial_\theta + F_1(\theta, y, v)\partial_y, \\ \mathcal{L}_2 &= F_2(\theta, y, v)\partial_\theta. \end{aligned} \tag{14}$$

Here we impose the periodic condition for $\phi(\theta, y, t)$ along y with period 1. Notice that $A(\theta, y) \ne 0$ when $\theta \notin [\theta_1, \theta_2]$. We easily know that the kernel space of $\mathcal{L}_0$ is one dimensional and given by $\mathcal{N}(\mathcal{L}_0) = \mathrm{span}\{1(y)\}$, where $1(y)$ represents a constant function with respect to y. Let $\mathcal{L}_0^*$ be the dual operator of $\mathcal{L}_0$, i.e.

$$\mathcal{L}_0^*\rho = -\partial_y(A(\theta, y)\rho).$$

Then by the Fredholm alternative, $\mathcal{L}_0$ also has a one-dimensional kernel space which is given $\mathcal{N}(\mathcal{L}_0^*) = \text{span}\{\rho^\infty\}$. ρ^∞ is obtained by solving the equation

$$\mathcal{L}_0^* \rho^\infty(y;\theta) = 0,$$

with periodic condition for y with period 1 and the condition $\int_{\mathbb{T}} \rho^\infty(y;\theta)\mathrm{d}y = 1$ where $\mathbb{T} = [0,1]$. Direct calculations give

$$\rho^\infty(y;\theta) = \frac{C_0(\theta)}{A(\theta,y)}, \tag{15}$$

where

$$C_0(\theta) = \Big(\int_{\mathbb{T}} \frac{1}{A(\theta,y)} \mathrm{d}y \Big)^{-1}. \tag{16}$$

It is easy to see that $\rho^\infty(\theta,\cdot)$ is a probability density function with respect to y.

Now we seek a solution to the backward Kolmogorov equation (13) in form of a multi-scale expansion

$$\phi = \phi_0 + \varepsilon\phi_1 + \mathcal{O}(\varepsilon^2).$$

By substituting the expansion into (13) and equating coefficients of successive powers of ε to zero yields the hierarchy

$$\mathcal{O}(\varepsilon^{-1}) \quad \mathcal{L}_0\phi_0 = 0, \tag{17}$$

$$\mathcal{O}(1) \quad \mathcal{L}_0\phi_1 = \frac{\partial\phi_0}{\partial t} - \mathcal{L}_1\phi_0. \tag{18}$$

From Equ. (17) and the property of $\mathcal{N}(\mathcal{L}_0)$, we know that ϕ_0 is a function independent of y. By the Fredholm alternative, the second equation (18) is solvable only when

$$\frac{\partial\phi_0}{\partial t} - \mathcal{L}_1\phi_0 \perp \text{Null}\{\mathcal{L}_0^*\}.$$

This implies that

$$\int_{\mathbb{T}} \rho^\infty(y;\theta)\Big(\frac{\partial\phi_0}{\partial t}(\theta,t) - B(\theta,y)\partial_\theta\phi_0(\theta,t)\Big)\mathrm{d}y = 0.$$

The equation can also be derived simply by multiplying (18) with ρ^∞ and integration in an period $[0,1)$. The equation can be further reduced to

$$\frac{\partial\phi_0}{\partial t} = \left(\int_{\mathbb{T}} \rho^\infty(y;\theta) B(\theta,y) \mathrm{d}y \right) \partial_\theta\phi_0(\theta,t).$$

It is the backward Kolmogrov equation for the following ordinary differential equation

$$\frac{\mathrm{d}\Theta}{\mathrm{d}t} = \int_{\mathbb{T}} B(\Theta,y)\rho^\infty(y;\Theta)\mathrm{d}y, \tag{19}$$

where ρ^∞ is given by (15). The equation (19) is the leading order approximation of the equation (9b). By the formula of B and ρ^∞, Equ. (19) can be rewritten as

$$\frac{\mathrm{d}\Theta}{\mathrm{d}t} = -g(\Theta)(C_0(\Theta) - v). \tag{20}$$

Here we used the fact that $\int_{\mathbb{T}} p(\theta, y)\mathrm{d}y = 0$ in Assumption (A1).

We then derive the time evolution of the contact point $x_{ct} = \varepsilon y_{ct}$. Notice that Eq. (9a) can be rewritten as

$$\frac{dx_{ct}}{dt} = A(\theta_a, y_{ct}) + \varepsilon F_1(\theta_a, y_{ct}, v), \tag{21}$$

which has the same structure as (9b). Similar derivations give the leading order approximation

$$\frac{dX}{dt} = \int_{\mathbb{T}} A(\Theta, y)\rho^{\infty}(y; \Theta)\mathrm{d}y = C_0(\Theta), \tag{22}$$

where we have used the formula of ρ^{∞}. The equation should be coupled with the equation (20) which gives the dynamics of Θ.

In summary, when $\theta_a \notin [\theta_0, \theta_1]$, the leading order approximation of (9) is given by

$$\frac{\mathrm{d}\Theta}{\mathrm{d}t} = -g(\Theta)(C_0(\Theta) - v), \tag{23a}$$

$$\frac{dX}{dt} = C_0(\Theta), \tag{23b}$$

where (Θ, X) approximates (θ_a, x_{ct}), $C_0(\theta)$ is defined in (16) representing the harmonic average of $A(\theta, y)$ in a period $\mathbb{T}$.

The equation (23) has a steady solution for the apparent contact angle Θ when

$$C_0(\Theta) = \Big(\int_{\mathbb{T}} \frac{1}{A(\Theta, y)}\mathrm{d}y \Big)^{-1} = v. \tag{24}$$

In this case, the contact line moves with a constant velocity v by the second equation of (23). One can easily see that the steady state solution Θ is a function of v. It can be verified that the function is not continuous around $v = 0$. Actually, notice that $A(\theta, y) = f(\theta, y)(\cos\theta_Y(y) - \cos(\theta + \theta_g(y)))$. We can expect that $\theta > \theta_2$ so that $A > 0$ when v is positive; and similarly $\theta < \theta_1$ so that $A < 0$ when v is negative. The different limits of the function when $v \to \pm 0$ corresponds to the contact angle hysteresis. Equ. (24) shows that the averaged apparent contact angle is determined by a harmonic average of $A(\cdot, \cdot)$ but independent of $B(\cdot, \cdot)$. Notice that the two examples in Section 2 have the same formula for A but not B. This implies that the averaged contact angle depends on the local geometric and chemical properties of the substrate, as well as the physical property of the fluid, but not on the specific setup of the wetting problem. In this sense, Equ. (24) can be applied to more general two-phase flow systems.

3.3. Rigorous results. We prove the asymptotic results in this subsection.

PROPOSITION 3.1. *Suppose that $\theta_a^{\varepsilon} \in [\theta_1, \theta_2]$ and $\eta(\theta) \in (0, 1]$ is the unique function satisfying $A(\theta, \eta(\theta)) = 0$ and $\partial_y A(\theta, \eta(\theta)) < -\lambda$ for some positive $\lambda > 0$. Let $(y_{ct}^{\varepsilon}, \theta_{ct}^{\varepsilon})$ be the solution of (9) and $(y_{ct}^{(0)}, \Theta)$ satisfies (12) with a proper k. We also assume that $\theta_{ct}^{\varepsilon}(0) = \Theta(0)$. Then there exist constants $K, c > 0$ such that*

$$|y_{ct}^{\varepsilon}(t) - y_{ct}^{(0)}(t)|^2 \le c(e^{-\lambda t/\varepsilon}|y_{ct}^{\varepsilon}(0) - y_{ct}^{(0)}(0)|^2 + \varepsilon^2)$$
$$|\theta_a^{\varepsilon}(t) - \Theta(t)|^2 \le ce^{Kt}(\varepsilon|y_{ct}^{\varepsilon}(0) - y_{ct}^{(0)}(0)|^2 + \varepsilon^2).$$

Proof. The proof is similar to that of Theorem 15.2 in [20]. Let $e(t) = y^\varepsilon_{ct}(t) - y^{(0)}_{ct}(t) = y^\varepsilon_{ct}(t) - k - \eta(\theta^\varepsilon_a(t))$. Then we have

$$\begin{aligned}\frac{de(t)}{dt} &= \frac{dy^\varepsilon_{ct}}{dt} - \eta'(\theta^\varepsilon_a)\frac{d\theta^\varepsilon_a}{dt}\\ &= \frac{1}{\varepsilon}A(\theta^\varepsilon_a, y^\varepsilon_{ct}) + F_1(\theta^\varepsilon_a, y^\varepsilon_{ct}, v) - \eta'(\theta^\varepsilon_a)(B(\theta^\varepsilon_a, y^\varepsilon_{ct}) + \varepsilon F_2(\theta^\varepsilon_a, y^\varepsilon_{ct}, t))\\ &= \frac{1}{\varepsilon}\Big(A(\theta^\varepsilon_a, y^\varepsilon_{ct}) - A(\theta^\varepsilon_a, k + \eta(\theta^\varepsilon_a))\Big) + F_1(\theta^\varepsilon_a, y^\varepsilon_{ct}, v)\\ &\quad - \eta'(\theta^\varepsilon_a)(B(\theta^\varepsilon_a, y^\varepsilon_{ct}) + \varepsilon F_2(\theta^\varepsilon_a, y^\varepsilon_{ct}, v)).\end{aligned}$$

In the last equation, we have used the fact that $A(\theta^\varepsilon_a, k + \eta(\theta^\varepsilon_a)) = A(\theta^\varepsilon_a, \eta(\theta^\varepsilon_a)) = 0$. We multiply the above inequality with $e(t)$ and obtain that

$$\begin{aligned}\frac{1}{2}\frac{de^2(t)}{dt} =& \frac{1}{\varepsilon}\Big(A(\theta^\varepsilon_a, y^\varepsilon_{ct}) - A(\theta^\varepsilon_a, k + \eta(\theta^\varepsilon_a))\Big)e(t)\\ &+ F_1(\theta^\varepsilon_a, y^\varepsilon_{ct}, v)e(t) - \eta'(\theta^\varepsilon_a)(B(\theta^\varepsilon_a, y^\varepsilon_{ct}) + \varepsilon F_2(\theta^\varepsilon_a, y^\varepsilon_{cy}, v))e(t).\end{aligned}$$

Notice that the assumption (A1) and the condition on η imply

$$\begin{aligned}&\Big(A(\theta^\varepsilon_a, y^\varepsilon_{ct}) - A(\theta^\varepsilon_a, k + \eta(\theta^\varepsilon_a))\Big)e(t)\\ =&\Big(A(\theta^\varepsilon_a, k + \eta(\theta^\varepsilon_a) + e(t)) - A(\theta^\varepsilon_a, k + \eta(\theta^\varepsilon_a))\Big)e(t) \le -\lambda e^2(t),\end{aligned}$$

and

$$|F_1(\theta^\varepsilon_a, y^\varepsilon_{ct}, v) - \eta'(\theta^\varepsilon_a)(B(\theta^\varepsilon_a, y^\varepsilon_{ct}) + \varepsilon F_2(\theta^\varepsilon_a, y^\varepsilon_{cy}, v))| \le c$$

for some positive number c.

By using the Cauchy-Schwartz inequality and choosing $\delta = \frac{\varepsilon}{\lambda}$, we have

$$\frac{1}{2}\frac{de^2(t)}{dt} \le -\frac{\lambda}{\varepsilon}e^2(t) + c|e(t)| \le -\frac{\lambda}{\varepsilon}e^2(t) + \frac{e^2(t)}{2\delta} + \frac{\delta c^2}{2} = -\frac{\lambda}{2\varepsilon}e^2(t) + \frac{\varepsilon c^2}{2\lambda}.$$

By Gronwall's lemma, we have

$$e^2(t) \le e^{-\frac{\lambda}{\varepsilon}t}e^2(0) + (1 - e^{-\frac{\lambda}{\varepsilon}t})\frac{\varepsilon^2 c^2}{\lambda^2}. \tag{25}$$

This gives the first estimate of the proposition.

Now we consider the approximation error to θ^ε_a. Set $e_\theta(t) = \theta^\varepsilon_a(t) - \Theta(t)$. By the equations (9) and (12), we have

$$\begin{aligned}\frac{de_\theta}{dt} &= B(\theta^\varepsilon_a, y^\varepsilon_{ct}) + \varepsilon F_2(\theta^\varepsilon_a, y^\varepsilon_{ct}, t) - vg(\Theta)\\ &= -g(\theta^\varepsilon_a)(1 + p(\theta^\varepsilon_a, y^\varepsilon_{ct}))A(\theta^\varepsilon_a, y^\varepsilon_{ct}) + vg(\theta^\varepsilon_a) + \varepsilon F_2(\theta^\varepsilon_a, y^\varepsilon_{ct}, v) - vg(\Theta)\\ &= -g(\theta^\varepsilon_a)(1 + p(\theta^\varepsilon_a, y^\varepsilon_{ct}))\Big(A(\theta^\varepsilon_a, y^\varepsilon_{ct}) - A(\theta^\varepsilon_a, k + \eta(\theta^\varepsilon_{ct}))\Big)\\ &\quad + v(g(\theta^\varepsilon_a) - g(\Theta)) + \varepsilon F_2(\theta^\varepsilon_a, y_{ct}\varepsilon, v),\end{aligned}$$

We multiply the above inequality by $e_\theta(t)$. By the smoothness of the related functions, we have

$$\frac{1}{2}\frac{de^2_\theta}{dt} = \frac{de_\theta}{dt}e_\theta(t) \le c|e(t)||e_\theta(t)| + c|e_\theta(t)|^2 + c\varepsilon|e_\theta| \le C(|e_\theta(t)|^2 + (|e(t)|^2 + \varepsilon^2)).$$

By using the Gronwall's inequality and noticing $e_\theta(0) = 0$, we obtain the second estimate of the proposition with $K = 2C$. ∎

When $\theta \notin [\theta_1, \theta_2]$, the function $A(\theta, y)$ do not equal to zero, then we have the following result.

PROPOSITION 3.2. *When $\theta \notin [\theta_1, \theta_2]$, under the assumptions (A1)-(A3), the solution of (9) converges uniformly to the solution of (23) as ε goes to zero if they start from the same initial values.*

Proof. The result is a direct conclusion of Theorem 14, P. 173 in [28]. ∎

THEOREM 3.1. *Assume the conditions (A1)-(A3) hold and v is small. Then the averaged dynamics of the (9) approaches to a steady state when t is large enough, where the averaged contact line position X and the averaged apparent contact angle Θ are given by*

$$\frac{dX}{dt} = v, \qquad \Big(\int_{\mathbb{T}} \frac{1}{A(\Theta, y)} \mathrm{d}y\Big)^{-1} - v = 0. \tag{26}$$

In addition, $\Theta(v)$ is discontinuous at $v = 0$, s.t.

$$\lim_{v \to 0^+} \Theta(v) \geq \theta_2 > \theta_1 \geq \lim_{v \to 0^-} \Theta(v).$$

Proof. We first consider the case when $v > 0$. If initially $\theta_a < \theta_1$, the averaged dynamics will be described by (23). Notice that

$$C_0 = \Big(\int_{\mathbf{T}} \frac{1}{A(\Theta, y)} dy\Big)^{-1} = \Big(\int_{\mathbf{T}} \frac{1}{f(\Theta, y)(\cos\theta_Y(y) - \cos(\Theta + \theta_g(y)))} dy\Big)^{-1}$$

Since $\Theta < \theta_1$ and $f(\Theta, y) \geq c_0 > 0$, we easily know that $C_0 < 0$. Then the equation $\frac{d\Theta}{dt} = -g(\Theta)(C_0 - v) \geq c_0 v > 0$, where we use the fact that $g(\Theta) \geq c_0 > 0$. Therefore, the contact angle will increase monotonously and will enter into the interval $[\theta_1, \theta_2]$.

If θ_a is in $[\theta_1, \theta_2]$, the averaged dynamics is described by (12). Since $g(\theta) > c_0 > 0$, we have $\frac{d\Theta}{dt} \geq c_0 v > 0$, then the apparent contact angle Θ will increase monotonously until it goes beyond θ_2.

When $\theta_a > \theta_2$, the averaged dynamics will again be determined by (23). Notice that $C_0 > 0$ in this case and $\lim_{\theta \to \theta_2^+} C_0(\theta) \downarrow 0$. Therefore when v is small enough, there exists a $\Theta > \theta_2$ such that $C_0(\Theta) = v$. This gives a steady state of the system.

Similar arguments can be done for the case when $v < 0$ which leads to a steady state with an apparent contact angle $\Theta < \theta_1$. This ends the proof of the theorem. ∎

4. Time averaging of the stochastic model. Similar to the deterministic case, we set $y_{ct} = \frac{x_{ct}}{\varepsilon}$ and reformulate the stochastic equation (8) to

$$\dot{y}_{ct} = \frac{1}{\varepsilon} A(\theta_a, y_{ct}) + \frac{1}{\sqrt{\varepsilon}} \alpha(\theta_a, y_{ct}) \dot{W} + F_1(\theta_a, y_{ct}, v), \tag{27a}$$

$$\dot{\theta}_a = B(\theta_a, y_{ct}) + \sqrt{\varepsilon} \beta(\theta_a, y_{ct}) \dot{W} + \varepsilon F_2(\theta_a, y_{ct}, v), \tag{27b}$$

where A, B, F_1 and F_2 are the same as in the deterministic case, $\alpha(\theta, y) = \sigma f(\theta, y)$ and $\beta(\theta, y) = -\sigma g(\theta, y)(1 + p(\theta, y)) f(\theta, y)$. We study the averaged dynamics of the stochastic system (27). We first derive the averaged equation by formal derivation and then prove the results rigorously.

4.1. Formal derivation. We will study the leading order approximation of (27) by using the backward Kolmogrov equation as in Section 3.2. The backward equation of (27) can be defined as,

$$\frac{\partial \phi}{\partial t} = \tilde{\mathcal{L}} \phi, \tag{28}$$

where the generator $\tilde{\mathcal{L}}$ is

$$\tilde{\mathcal{L}} = (B + \varepsilon F_2)\partial_\theta + (\varepsilon^{-1}A + F_1)\partial_y + \frac{1}{2}\left(\varepsilon\beta^2\partial_{\theta\theta} + 2\alpha\beta\partial_{\theta y} + \varepsilon^{-1}\alpha^2\partial_{yy}\right) \tag{29}$$

Notice that the operator can be expanded as $\tilde{\mathcal{L}} = \varepsilon^{-1}\tilde{\mathcal{L}}_0 + \tilde{\mathcal{L}}_1 + \varepsilon\tilde{\mathcal{L}}_2$ with

$$\begin{aligned}
\tilde{\mathcal{L}}_0 &= A\partial_y + \frac{1}{2}\alpha^2\partial_{yy} \\
\tilde{\mathcal{L}}_1 &= B\partial_\theta + \alpha\beta\partial_{\theta y} + F_1\partial_y \\
\tilde{\mathcal{L}}_2 &= \frac{1}{2}\beta^2\partial_{\theta\theta} + F_2\partial_\theta.
\end{aligned}$$

We seek a solution ϕ of the backward equation (28) in the form of the multi-scale expansion that

$$\phi = \phi_0 + \varepsilon\phi_1 + \varepsilon^2\phi_2 + \mathcal{O}(\varepsilon^3).$$

Substitute the equation into (28) and equate coefficients of powers of ε to zero. We derive

$$\mathcal{O}(\varepsilon^{-1}) \quad \tilde{\mathcal{L}}_0\phi_0 = 0 \tag{30}$$

$$\mathcal{O}(1) \qquad \tilde{\mathcal{L}}_0\phi_1 = \frac{\partial\phi_0}{\partial t} - \tilde{\mathcal{L}}_1\phi_0 \tag{31}$$

$$\mathcal{O}(\varepsilon) \qquad \tilde{\mathcal{L}}_0\phi_2 = \frac{\partial\phi_1}{\partial t} - \tilde{\mathcal{L}}_1\phi_1 - \tilde{\mathcal{L}}_2\phi_0 \tag{32}$$

Let $\tilde{\mathcal{L}}_0^*$ be the adjoint operator. Then for each fixed θ, one can verify that $\tilde{\mathcal{L}}_0$ satisfies the ergodicity condition, i.e. both $\tilde{\mathcal{L}}_0$ and $\tilde{\mathcal{L}}_0^*$ have a one-dimensional null space characterized by

$$\tilde{\mathcal{L}}_0 1(y) = 0, \tag{33}$$

$$\tilde{\mathcal{L}}_0^*\rho^\infty(y;\theta) = 0, \quad \int_{\mathbb{T}} \rho^\infty \mathrm{d}y = 1, \tag{34}$$

where the operator $\tilde{\mathcal{L}}_0$ and $\tilde{\mathcal{L}}_0^*$ are equipped with periodic boundary conditions in y. Then the equation (30) implies that ϕ_0 is in the null space of $\mathcal{L}_0$, i.e. ϕ_0 is independent of y. By the Fredholm alternative for (31), viewed as a differential equation in y, we see that

$$\frac{\partial\phi_0}{\partial t} - \tilde{\mathcal{L}}_1\phi_0 \perp \mathrm{Null}\{\tilde{\mathcal{L}}_0^*\}.$$

This implies that

$$\int_{\mathbb{T}} \frac{\partial\phi_0}{\partial t}\rho^\infty(y;\theta) - B(\theta,y)\partial_\theta\phi_0\rho^\infty(y;\theta)\mathrm{d}y = 0.$$

Notice that ρ^∞ is a probability density, we have

$$\frac{\partial\phi_0}{\partial t} = \left(\int_{\mathbb{T}} B(\theta,y)\rho^\infty(y;\theta)\mathrm{d}y\right)\partial_\theta\phi_0.$$

It is the backward equation of the following deterministic differential equation,

$$\frac{\mathrm{d}\Theta}{\mathrm{d}t} = \int_{\mathbb{T}} B(\Theta, y)\rho^{\infty}(y;\Theta)\mathrm{d}y, \quad \Theta(0) = \theta_0. \tag{35}$$

Here ρ^{∞} is solved from (34). Actually, we have the explicit formula of the probability density ρ^{∞} that

$$\rho^{\infty} = C\exp\Big(-\int_0^y \frac{2(\alpha\alpha' - A)}{\alpha^2}\mathrm{d}y\Big)\Big[D + \int_0^y \frac{2}{\alpha^2}\exp\Big(\int_0^{\tilde{y}} \frac{2(\alpha\alpha' - A)}{\alpha^2}\mathrm{d}\bar{y}\Big)\mathrm{d}\tilde{y}\Big], \tag{36}$$

where

$$D = \Big[\exp\Big(\int_{\mathbb{T}} \frac{2(\alpha\alpha' - A)}{\alpha^2}\mathrm{d}y\Big) - 1\Big]^{-1}\int_{\mathbb{T}} \frac{2}{\alpha^2}\exp\Big(\int_0^y \frac{2(\alpha\alpha' - A)}{\alpha^2}\mathrm{d}\bar{y}\Big)\mathrm{d}y,$$

$$C = \Big[\int_{\mathbb{T}} \exp\Big(-\int_0^y \frac{2(\alpha\alpha' - A)}{\alpha^2}\mathrm{d}\bar{y}\Big)\Big(D + \int_0^y \frac{2}{\alpha^2}\exp\Big(\int_0^{\tilde{y}} \frac{2(\alpha\alpha' - A)}{\alpha^2}\mathrm{d}\bar{y}\Big)\mathrm{d}\tilde{y}\Big)\mathrm{d}y\Big]^{-1}.$$

Similarly, for the contact point $\tilde{x}_{ct} = \varepsilon\tilde{y}_{ct}$, we can derive its leading order approximation which is given by

$$\frac{dX}{dt} = \int_{\mathbb{T}} A(\Theta, y)\rho^{\infty}(\Theta, y)\mathrm{d}y, \quad X(0) = x_0. \tag{37}$$

The equation should be coupled with (35).

In summary, the leading order approximation of the stochastic equation (27) is given by the equations (35) and (37). In steady state, the averaged apparent contact angle will be given by

$$\int_{\mathbb{T}} B(\Theta, y)\rho^{\infty}(y;\Theta)\mathrm{d}y = 0$$

By the the formula for B, it is rewritten as

$$\int_{\mathbb{T}} (1 + p(\Theta, y))f(\Theta, y)(\cos\theta_Y(y) - \cos(\Theta + \theta_g(y)))\rho^{\infty}(y;\Theta)\mathrm{d}y = v. \tag{38}$$

It characterizes the averaged dynamic contact angles in steady states. Direct computations show that the averaged dynamics by (35) generates contact angle hysteresis phenomena and (38) gives an explicit formula for the averaged advancing and receding contact angles. This will also be shown by numerical examples in Section 5.

4.2. Rigorous Results. We present a rigorous result for the multi-scale analysis in the previous subsection. The proof of the theorem follows that of Theorem 17.1 in [20].

THEOREM 4.1. *Assume the conditions (A1)-(A3) hold. Let $p > 1$ and $\Theta(0) = \theta_0, X(0) = \tilde{x}_{ct}(0)$. Then the function $\tilde{\theta}(t)$ which solving (27) converges to $\Theta(t)$ solving (35) in the sense that : for any $T > 0$, there is $C_1 = C_1(T)$ such that*

$$\mathbb{E}\Big(\sup_{0\le t\le T} |\tilde{\theta}_a(t) - \Theta(t)|^p\Big) \le C_1\varepsilon^{p/2}. \tag{39}$$

Similarly, the contact point $\tilde{x}_{ct} = \varepsilon\tilde{y}_{ct}$ converges to $X(t)$ solving (37) in the sense that: for any $T > 0$, there is $C_2 = C_2(T)$ such that

$$\mathbb{E}\Big(\sup_{0\le t\le T} |\tilde{x}_{ct}(t) - X(t)|^p\Big) \le C_2\varepsilon^{p/2}. \tag{40}$$

Proof. Let $H(\theta) = \int_{\mathbb{T}} B(\theta, y)\rho^{\infty}(y;\theta)\mathrm{d}y$. Since $\tilde{\mathcal{L}}_0$ is a differential operator in y only; θ appears as a parameter, we can construct an elliptic boundary value problem:

$$\begin{aligned}
&\tilde{\mathcal{L}}_0\phi(\theta, y) = B(\theta, y) - H(\theta)\\
&\int_{\mathbb{T}} \phi(\theta, y)\rho^{\infty}(y;\theta)\mathrm{d}y = 0\\
&\phi(\theta, \cdot) \text{ is periodic on } \mathbb{T}.
\end{aligned}$$

Due to the condition of $B(\theta, y)$, we know that the function $H(\theta)$ is smooth and periodic in θ. Hence ϕ and all its derivatives are smooth and periodic.

By construction we have

$$\int_{\mathbb{T}} (B(\theta, y) - H(\theta))\rho^{\infty}(y;\theta)\mathrm{d}y = 0$$

and ρ^{∞} spans $N(\tilde{\mathcal{L}}_0^*)$. Hence, by the Fredholm alternative, ϕ has an unique solution.

Notice that the generator for (27) is

$$\tilde{\mathcal{L}} = \varepsilon^{-1}\tilde{\mathcal{L}}_0 + \tilde{\mathcal{L}}_1 + \varepsilon\tilde{\mathcal{L}}_2$$

Now we apply the Ito formula to $\phi(\theta(t), y(t))$ to obtain the following informal expression [20], with precise interpretation found by integrating in time:

$$\begin{aligned}
\frac{\mathrm{d}\phi}{\mathrm{d}t} &= \tilde{\mathcal{L}}\phi + \sqrt{\varepsilon}\partial_\theta\phi\beta\dot{W} + \frac{1}{\sqrt{\varepsilon}}\partial_y\phi\alpha\dot{W}\\
&= \varepsilon^{-1}\tilde{\mathcal{L}}_0\phi + \tilde{\mathcal{L}}_1\phi + \varepsilon\tilde{\mathcal{L}}_2\phi + \sqrt{\varepsilon}\partial_\theta\phi\beta\dot{W} + \frac{1}{\sqrt{\varepsilon}}\partial_y\phi\alpha\dot{W}
\end{aligned}$$

Since $\tilde{\mathcal{L}}_0\phi = B(\theta, y) - H(\theta)$, we obtain

$$\begin{aligned}
\frac{\mathrm{d}\theta}{\mathrm{d}t} &= B(\theta, y) + \varepsilon F_2(\theta, y, t) + \sqrt{\varepsilon}\beta(\theta, y)\dot{W}\\
&= H(\theta) + \varepsilon(\frac{\mathrm{d}\phi}{\mathrm{d}t} - \tilde{\mathcal{L}}_1\phi + F_2) - \varepsilon^2\tilde{\mathcal{L}}_2\phi + \sqrt{\varepsilon}(\beta - \partial_y\phi\alpha)\dot{W} - \varepsilon\sqrt{\varepsilon}\partial_\theta\phi\beta\dot{W} \qquad (41)
\end{aligned}$$

The function B, F_2, ϕ and its derivatives are smooth and bounded. Set

$$\begin{aligned}
h_1(t) &= \int_0^t \frac{\mathrm{d}\phi}{\mathrm{d}t} - \tilde{\mathcal{L}}_1\phi + F_2\mathrm{d}t\\
&= (\phi(\theta(t), y(t)) - \phi(\theta(0) - y(0))) - \int_0^t B\partial_\theta\phi + \alpha\beta\partial_\theta\partial_y\phi + F_1\partial_y\phi + F_2\mathrm{d}s
\end{aligned}$$

and

$$h_2(t) = -\int_0^t \tilde{\mathcal{L}}_2\phi\mathrm{d}s = -\int_0^t \frac{1}{2}\beta^2\partial_\theta\partial_\theta\phi + F_2\partial_\theta\phi\mathrm{d}s.$$

Then there exists a constant $C > 0$ such that

$$\sup_{0\le t\le T} |h_1(t)| \le C, \quad \sup_{0\le t\le T} |h_2(t)| \le C$$

Now consider the martingale terms

$$M_1(t) = -\int_0^t (\alpha\partial_y\phi - \beta)\mathrm{d}W \qquad \text{and} \qquad M_2(t) = -\int_0^t \beta\partial_\theta\phi\mathrm{d}W.$$

Since $\partial_y\phi, \partial_\theta\phi, \beta, \alpha$ are bounded and smooth, the Ito isometry gives

$$\mathbb{E}|\langle M_1\rangle_t| \le \int_0^t \mathbb{E}(|(\alpha\partial_y\phi - \beta)|_F^2)\mathrm{d}s = \int_0^t \mathbb{E}(|M_1(t)|^2)\mathrm{d}s \le C_1 t.$$

Similarly, for $p \ge 1$,

$$\mathbb{E}|\langle M_1\rangle_t|^{p/2} \le C_1.$$

We can get the similar result of $M_2(t)$:

$$\mathbb{E}|\langle M_2\rangle_t| \le C_1 t, \quad \mathbb{E}|\langle M_2\rangle_t|^{p/2} \le C_1$$

Notice that $H(\theta)$ is a Lipschitz function, then the rigorous interpretation of (41) is

$$\theta(t) = \theta(0) + \int_0^t H(\theta(s))\mathrm{d}s + \varepsilon h_1(t) + \varepsilon^2 h_2(t) + \sqrt{\varepsilon}M_1(t) + \varepsilon\sqrt{\varepsilon}M_2(t).$$

We also have

$$\Theta(t) = \Theta(0) + \int_0^t H(\Theta(s))\mathrm{d}s$$

Let $e(t) = \theta(t) - \Theta(t)$, and $e(0) = 0$,

$$|e(t)| \le \int_0^t L|e(s)|\mathrm{d}s + \varepsilon C_1 + \varepsilon^2 C_1 + \sqrt{\varepsilon}|M_1(t)| + \varepsilon\sqrt{\varepsilon}|M_2(t)|.$$

Hence, by the Burkholder-Davis-Gundy inequality [20], we obtain

$$\begin{aligned}\mathbb{E}(\sup_{0\le t\le T}|e(t)|^p) &\le C_1(\varepsilon^2 + \varepsilon^{2p} + \varepsilon^{p/2}\mathbb{E}|\langle M_1\rangle_t|^{p/2} + \varepsilon^{3p/2}\mathbb{E}|\langle M_2\rangle_t|^{p/2} \\ &\quad + L^p T^{p-1}\int_0^T \mathbb{E}(|e(s)|^p)\mathrm{d}s) \\ &\le C_1(\varepsilon^{p/2} + \int_0^T \mathbb{E}(\sup_{0\le\tau\le s}|e(\tau)|^p)\mathrm{d}s)\end{aligned}$$

By Gronwall inequality, we deduce that

$$\mathbb{E}(\sup_{0\le t\le T}|e(t)|^p) \le C_1\varepsilon^{p/2}.$$

This is the estimate in (39). The proof on the convergence of the dynamics of the contact point (i.e. (40)) is similar (even simpler) and we ignore it. ∎

4.3. Convergence of the stochastic system to the deterministic system. In this subsection, we want to show that the averaging stochastic dynamics (35) converges to that of the deterministic averaged dynamics (12) and (20) when the

noise level $\sigma \to 0$. To this end, we need to consider two different cases: i) $A > 0$ or $A < 0$ always holds; ii) there exists at least one y_0 such that $A(\Theta, y_0) = 0$. Since $f(\Theta, y) > 0$ always holds due to the fact that $\theta_g < 90°$, it is obvious that the first case occurs when $\Theta \notin [\theta_1, \theta_2]$, while the second case occurs when $\Theta \in [\theta_1, \theta_2]$.

Case i): We first assume that $A(\Theta, y) < 0$ always holds for all $y \in \mathbb{T}$. It is sufficient to prove that the invariant measure (36) of the stochastic system converges to the invariant measure (15) of the deterministic system. For simplicity, we will omit the dependence of all the functions on Θ.

Denoting $V(y) = -\int_0^y \frac{2A}{f^2} \mathrm{d}y$, which is positive and strictly monotonically increasing in y, we can rewrite the invariant measure (36) as

$$C^{-1}\rho_\sigma^\infty = \Big(\frac{f(y)}{f(0)}\Big)^{-2} e^{-\frac{V(y)}{\sigma^2}} \Big\{ \frac{1}{e^{\frac{V(1)}{\sigma^2}} - 1} Q(1) + Q(y) \Big\}, \tag{42}$$

where $Q(y) = \int_0^y \frac{2}{\sigma^2 f^2(0)} e^{\frac{V(\tilde{y})}{\sigma^2}} \mathrm{d}\tilde{y}$. Due to the monotonicity of $V(\tilde{y})$, we can apply the change of variable $\tilde{z} = V(y) - V(\tilde{y})$. Then $Q(y)$ (for $0 < y \leqslant 1$) can be further simplified as

$$\begin{aligned} Q(y) &= -e^{\frac{V(y)}{\sigma^2}} \int_0^{V(y)} \frac{f^2(V^{-1}(V(y) - \tilde{z}))}{\sigma^2 f^2(0) A(V^{-1}(V(y) - \tilde{z}))} e^{-\frac{\tilde{z}}{\sigma^2}} \mathrm{d}\tilde{z} \\ &= e^{\frac{V(y)}{\sigma^2}} \Big(-\frac{f^2(y)}{f^2(0)A(y)} + O(\sigma^2) \Big), \end{aligned} \tag{43}$$

where we have used Watson' lemma (or simply an integration by parts) to deduce the leading order behavior in the second equality. Putting this estimate into (42), we find that

$$C^{-1}\rho_\sigma^\infty = -\frac{1}{A(y)} + O(\sigma^2) + \Big(\frac{f(y)}{f(0)}\Big)^{-2} \frac{e^{\frac{V(1)-V(y)}{\sigma^2}}}{e^{\frac{V(1)}{\sigma^2}} - 1} (-\frac{1}{A(0)} + O(\sigma^2)),$$

which converges to $-\frac{1}{A(y)}$ as $\sigma^2 \to 0$ for any $0 < y \leqslant 1$. In fact, we can show that for any function $\zeta(y) \in C^\infty(\mathbb{T})$, $\lim_{\sigma\to 0} \int_0^1 \zeta(y) C^{-1}\rho_\sigma^\infty(y) \mathrm{d}y = -\int_0^1 \frac{\zeta(y)}{A(y)} \mathrm{d}y$. This is easily seen by noticing that $\int_0^1 \left(\frac{f(y)}{f(0)}\right)^{-2} \zeta(y) e^{-\frac{V(y)}{\sigma^2}} \mathrm{d}y = -\frac{f^2(0)\zeta(0)}{2A(0)}\sigma^2 + O(\sigma^4)$ using Watson's lemma. Taking $\zeta \equiv 1$, we obtain that $C^{-1} \to -\int_0^1 \frac{\mathrm{d}y}{A(y)}$ as $\sigma \to 0$. As a result, the right side of (35) converges to that of (20). Moreover, we have the pointwise (and weak) convergence in $\mathbb{T}$:

$$\lim_{\sigma\to 0} \rho_\sigma^\infty(y) = \frac{1}{A(y)} \Big(\int_0^1 \frac{\mathrm{d}y}{A(y)} \Big)^{-1}. \tag{44}$$

When $A < 0$, by change of variables $\bar{y} = 1 - y$ and $\bar{A} = -A > 0$, we can rewrite the equation for the invariant measure as $\tilde{\mathcal{L}}_0^* \rho^\infty(\bar{y}; \theta) = 0$ so that ρ^∞ is represented using $\bar{y}$ and $\bar{A} > 0$ instead of y and A. Thus the previous argument can still apply.

Case ii): We first make an assumption that for the periodic function $A(y)$, there are two zeros y_1 and y_0 in $[0, 1)$ such that $A'(y_1) > 0$ and $A'(y_0) < 0$, i.e., y_1 is an unstable equilibrium for the fast deterministic dynamics (9a) while y_0 is an asymptotically stable equilibrium. Due to the periodicity of A, we can assume $y_1 = 0$ and $y_0 \in (0, 1)$ without loss of generality. These assumptions hold for our choices of θ_Y in the numerical examples.

We introduce $V(y) = -\int_{y_0}^{y} \frac{2A}{f^2} \mathrm{d}y$, which now plays the role of potential function in the fast dynamics (9a) or (27). Then V is strictly monotonically decreasing in $(0, y_0)$ and strictly monotonically increasing in $(y_0, 1)$. In particular, it achieves its maxima at $y = 0$ and $y = 1$ while it has a minimum at $y = y_0$, i.e., $V'(0) = V'(1) = 0$, $V''(0) = V''(1) < 0$, $V(y_0) = V'(y_0) = 0$, $V''(y_0) > 0$. For our convenience, we rewrite the invariant measure (36) by using a different integrating factor as

$$C^{-1}\rho_\sigma^\infty = \Big(\frac{f(y)}{f(y_0)}\Big)^{-2} e^{-\frac{V(y)}{\sigma^2}} \Big\{ \frac{e^{\frac{V(0)}{\sigma^2}}}{e^{\frac{V(1)}{\sigma^2}} - e^{\frac{V(0)}{\sigma^2}}} Q(1) - \frac{e^{\frac{V(1)}{\sigma^2}}}{e^{\frac{V(1)}{\sigma^2}} - e^{\frac{V(0)}{\sigma^2}}} Q(0) + Q(y) \Big\} \tag{45}$$

where $Q(y) = \int_{y_0}^{y} \frac{2}{\sigma^2 f^2(y_0)} e^{\frac{V(\tilde{y})}{\sigma^2}} \mathrm{d}\tilde{y}$.

We claim that for any function $\zeta(y) \in C^\infty(\mathbb{T})$, $\lim_{\sigma\to 0} \int_0^1 \zeta(y)\rho_\sigma^\infty(y)\mathrm{d}y = \zeta(y_0)$. For this purpose, we need to estimate the quantities $Q(0)$, $Q(1)$, $\int_0^1 \zeta(y)\Big(\frac{f(y)}{f(y_0)}\Big)^{-2} e^{-\frac{V(y)}{\sigma^2}} \mathrm{d}y$, and $\int_0^1 \zeta(y)\Big(\frac{f(y)}{f(y_0)}\Big)^{-2} e^{-\frac{V(y)}{\sigma^2}} Q(y)\mathrm{d}y$.

By using Laplace method near $\tilde{y} = 0$, we can estimate $Q(0)$ as

$$Q(0) = -\frac{2e^{\frac{V(0)}{\sigma^2}}}{\sigma^2 f^2(y_0)} \int_0^{y_0} e^{\frac{V(\tilde{y})-V(0)}{\sigma^2}} \mathrm{d}\tilde{y} = -\frac{2e^{\frac{V(0)}{\sigma^2}}}{\sigma^2 f^2(y_0)} \Big(\frac{\sqrt{\pi}\sigma}{\sqrt{-2V''(0)}} + o(\sigma) \Big).$$

In the same way, $Q(1)$ can be estimated as

$$Q(1) = \frac{2e^{\frac{V(1)}{\sigma^2}}}{\sigma^2 f^2(y_0)} \Big(\frac{\sqrt{\pi}\sigma}{\sqrt{-2V''(1)}} + o(\sigma) \Big).$$

By using Laplace method near $\tilde{y} = y_0$, we obtain the following estimate

$$\int_0^1 \zeta(y)\Big(\frac{f(y)}{f(y_0)}\Big)^{-2} e^{-\frac{V(y)}{\sigma^2}} \mathrm{d}y = \zeta(y_0)\Big(\frac{\sqrt{2\pi}\sigma}{\sqrt{V''(y_0)}} + o(\sigma) \Big).$$

For the last integral, we can bound it by an $O(\frac{1}{\sigma^2})$ term:

$$\Big| \int_0^1 \zeta(y)\Big(\frac{f(y)}{f(y_0)}\Big)^{-2} e^{-\frac{V(y)}{\sigma^2}} Q(y)\mathrm{d}y \Big| \leqslant \frac{2}{\sigma^2} \int_0^1 \Big| \frac{\zeta(y)}{f^2(y)} \Big| \mathrm{d}y,$$

where we have used $V(\tilde{y}) \leqslant V(y)$ for any $\tilde{y}$ between y_0 and y to bound the exponential term.

To sum up, we have from (45) that

$$\int_0^1 \zeta(y) C^{-1}\rho_\sigma^\infty(y)\mathrm{d}y = \zeta(y_0) \frac{e^{\frac{V(0)+V(1)}{\sigma^2}}}{e^{\frac{V(1)}{\sigma^2}} - e^{\frac{V(0)}{\sigma^2}}} \Big(\frac{2\pi f(0)}{f(y_0)\sqrt{-A'(0)A'(y_0)}} + o(1) \Big) + O(\frac{1}{\sigma^2}),$$

whose leading order term is $O(\exp(\frac{\min\{V(0),V(1)\}}{\sigma^2}))$ with an exponential growth as $\sigma \to 0$. In particular, when $\zeta \equiv 1$, this implies that

$$C^{-1} = \int_0^1 C^{-1}\rho_\sigma^\infty(y)\mathrm{d}y = \frac{e^{\frac{V(0)+V(1)}{\sigma^2}}}{e^{\frac{V(1)}{\sigma^2}} - e^{\frac{V(0)}{\sigma^2}}} \Big(\frac{2\pi f(0)}{f(y_0)\sqrt{-A'(0)A'(y_0)}} + o(1) \Big) + O(\frac{1}{\sigma^2}).$$

Combining these two estimates together, we arrive at our claim. Moreover, $\rho_\sigma^\infty(y)$ weakly converges to $\delta(y - y_0)$. Taking $\zeta(y) = B(\Theta, y)$, we immediately obtain that the right side of (35) converges to that of (12).

5. Numerical examples. In this section, we present some numerical examples for the deterministic model (9), the stochastic model (27) and their averaged systems. We apply the forward Euler method to numerically solve the ordinary differential equations and use the Milstein method to solve the stochastic system (27).

Example 1. We consider the problem for a fiber moving in a liquid reservoir described in Section 2.1. The surface of the fiber is given by $R(x,t) = R_0 + \varepsilon R_1((x - vt)/\varepsilon)$, with $R_0 = 0.1$ and $R_1(y) = \sin(2\pi y)/4$. For the Young's angle, we set $\theta_Y(y) = \pi/2 + \pi/12\sin(2\pi y)$. We solve the equation (5) by setting $\alpha = 0$, $\zeta = 100$, $\gamma/\mu = 1$ and $r_c = 10$.

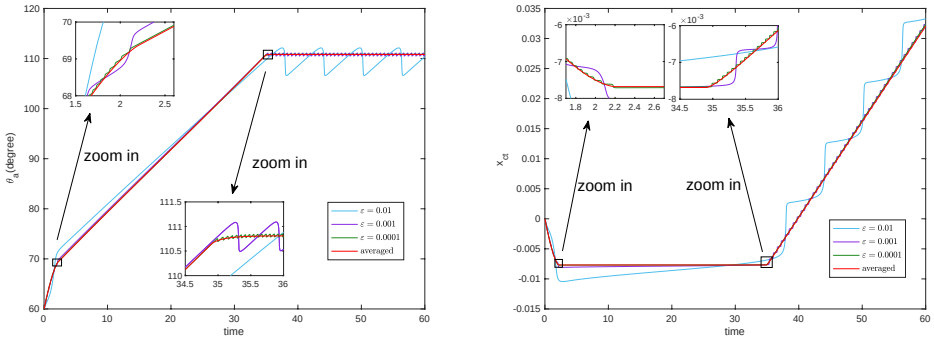

FIG. 3. *Advancing dynamics for* $\varepsilon = 0.05, 0.01, 0.001$ *and* 0.0001 *and the averaged contact angle and contact point with velocity* $v_w = -0.01$. *Left panel: The dynamical contact angle starting from* $\theta_{init} = 60°$. *Right panel: The contact line position starting form* 0.

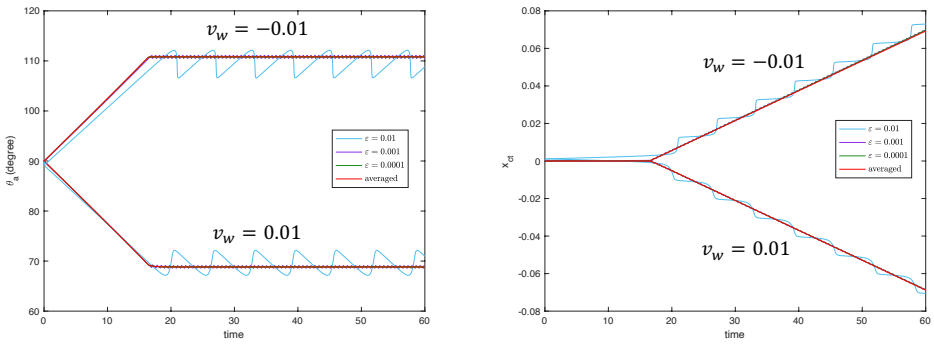

FIG. 4. *Receding and advancing dynamics for* $\varepsilon = 0.1, 0.01, 0.001$ *and* 0.0001 *and their respective averaged contact angle and contact point with the wall velocity* $v_w = \pm 0.01$. *Left panel: The dynamical contact angle starting from* $\theta_{init} = 90°$. *Right panel: The contact line position starting form* 0.

We first did experiments for several choices of ε with the initial contact angle $\theta_a = 60°$ and the initial contact point $x_{ct} = 0$. We choose $v_w = -0.01$ for the fiber velocity, which corresponds an advancing contact line with velocity $v = -v_w = 0.01$ in (7). The numerical results are shown in Figure 3. We observe that the advancing contact angle and corresponding contact point have a clear three-stage process. From the left subfigure, we can see that there exist two critical values $\theta_1 \approx 69.2°$ and

$\theta_2 \approx 110.7^\circ$ for the dynamic contact angle. In the first stage that the contact angle is smaller than θ_1, the solutions of Equ. (5) converge to that of the averaged equation (23) when ε goes to zero. In the second stage that the contact angle is between θ_1 and θ_2, the solutions of Equ. (5) converge to that of the averaged system (12). The contact angle increases monotonously in the first two stages. In the third stage, the solutions of Equ. (5) again converge to that of the averaged system (23). In particular, the contact angles oscillate around a value which corresponds to the steady state of (23), which is actually characterized by Equ. (24). All the observations are consistent with our analysis in Section 3.

To see the contact angle hysteresis, we did more tests by setting the velocity of the fiber as $v_w = \pm 0.01$. Here we choose the initial contact angle as $\theta_a = 90^\circ$. The numerical results are illustrated in Figure 4. Once again we observe the convergence of the solutions of the system (5) to that of the corresponding averaged equations. Furthermore, the averaged advancing contact angle is clearly much larger than the receding one in steady states. Both of them can be described by Equ. (24) (noticing the contact line velocity is opposite to the fiber velocity $v = -v_w$). This verifies the analytical results in Theorem 3.1.

Example 2. We consider the fiber motion in a liquid as in Example 1 with an extra stochastic force term as in (8). We set the initial contact angle $\theta_a = 90^\circ$, the noise coefficient $\sigma = 0.1, 0.3, 0.6, 0.8$, and all other conditions are the same as in the previous example. The numerical results are shown in Figure 5. We only show the dynamics of the contact angles since the plots on the contact points are similar to those in deterministic case. We can see that the numerical solutions of (8) converge to that of the averaged equation (35)(red curves) in all the four cases. The contact angle hysteresis is clearly observed. Furthermore, the contact angles in steady state are affected by the value of σ. When σ becomes smaller, the averaged dynamics of the stochastic system is much closer to that of the deterministic system. This verifies the analysis in Section 4.

Example 3. We consider the imbibition of liquid channel with smoothly oscillating boundary as described in Section 2.2. The boundary is given by $h(x,t) = h_0 + \varepsilon h_1((x+vt)/\varepsilon)$ with $h_0 = 0.8$ and $h_1 = \sin(2\pi y)/4$. The Young's angle is $\theta_Y(y) = \pi/3 + \pi/20 \sin(2\pi y)$. In the ODE system (6), we set $\alpha = 0, \xi = 100$ and $\gamma/\mu = 1$. We did experiments for several choices of ε with the initial contact angle $\theta_a = 60^\circ$ and the initial contact point $x_{ct} = 0$. We set the velocity $v = \pm 0.01$ which respectively correspond to the advancing and receding motion of the contact line. The numerical results are shown in Figure 6. We observe that the dynamics by (6) converges to the averaged system (12) and (23) in both the advancing and receding cases, similar to that in Example 1.

Example 4. We study the corresponding stochastic model for the liquid imbibition problem in a channel. We will solve the SDE model (8). We set the noise coefficient $\sigma = 0.1, 0.3, 0.6, 0.8$, and all other conditions are the same as the previous example. The numerical results on the dynamic contact angles are shown in Figure 7. Once again, we observe the convergence of the solutions of the stochastic equation to those of Equ. (35) with decreasing ε. When the coefficient σ is small, the averaged dynamics of the stochastic system is close to that of the deterministic one.

Example 5. In the last example, we will study the velocity dependence of the dynamic contact angle hysteresis on the velocity. We solve the stochastic systems for both the moving fiber problem (as in Example 2) and the liquid imbibition problem (as in Example 4). We set $\varepsilon = 0.001$, $\sigma = 0.1$, and choose different velocity v. The left subplot in Figure 8 describes the dynamics of the advancing and receding contact

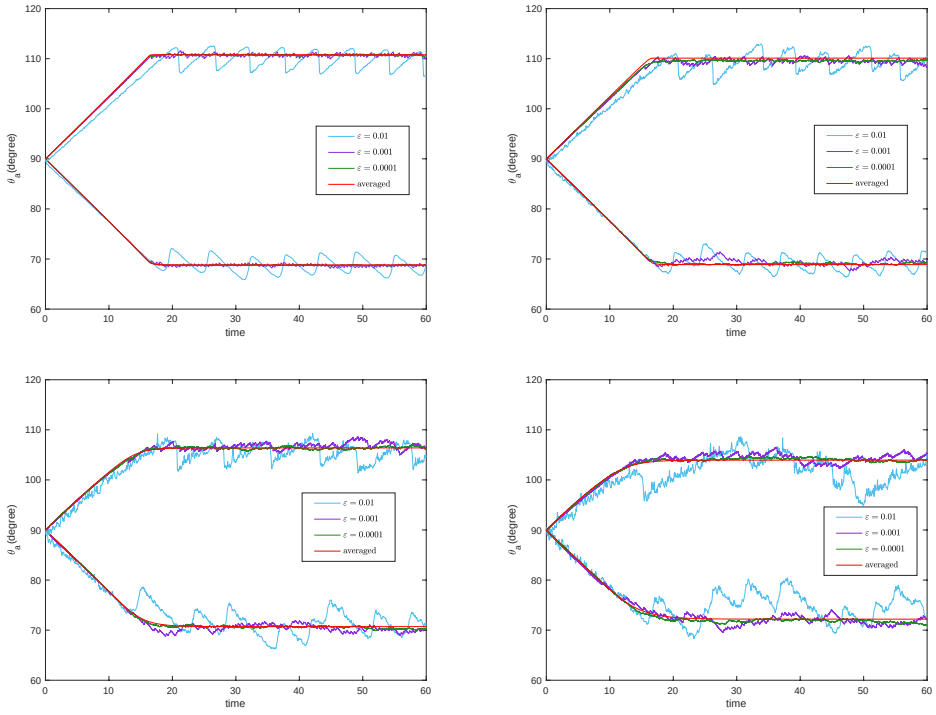

FIG. 5. *Receding and advancing dynamics for* $\varepsilon = 0.05, 0.01, 0.001$ *and* 0.0001 *and the averaged contact angle. Upper left panel:* $\sigma = 0.1$. *Upper right panel:* $\sigma = 0.3$. *Lower left panel:* $\sigma = 0.6$. *Lower right panel:* $\sigma = 0.8$.

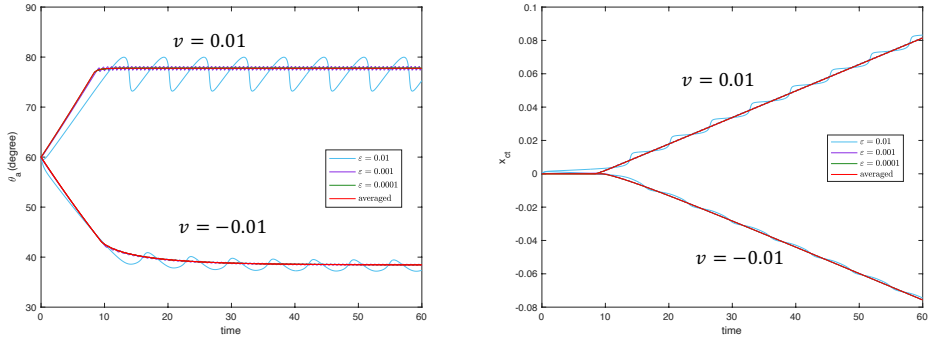

FIG. 6. *Receding and advancing dynamics for* $\varepsilon = 0.05, 0.01, 0.001$ *and* 0.0001 *and their respective averaged contact angle and contact point with velocity* $v = \pm 0.01$. *Left panel: The dynamical contact angle starting from* $\theta_{init} = 60°$. *Right panel: The contact line position starting form* 0.

angles for different contact line velocity on a fiber. We see clearly the asymmetric dependence of the advancing and receding contact angles on the velocity. This is consistent of the experimental observations in [15]. Interestingly, similar phenomena are observed for the channel case as shown in the right subplot in Figure 8. More discussions on such phenomena are referred to [39].

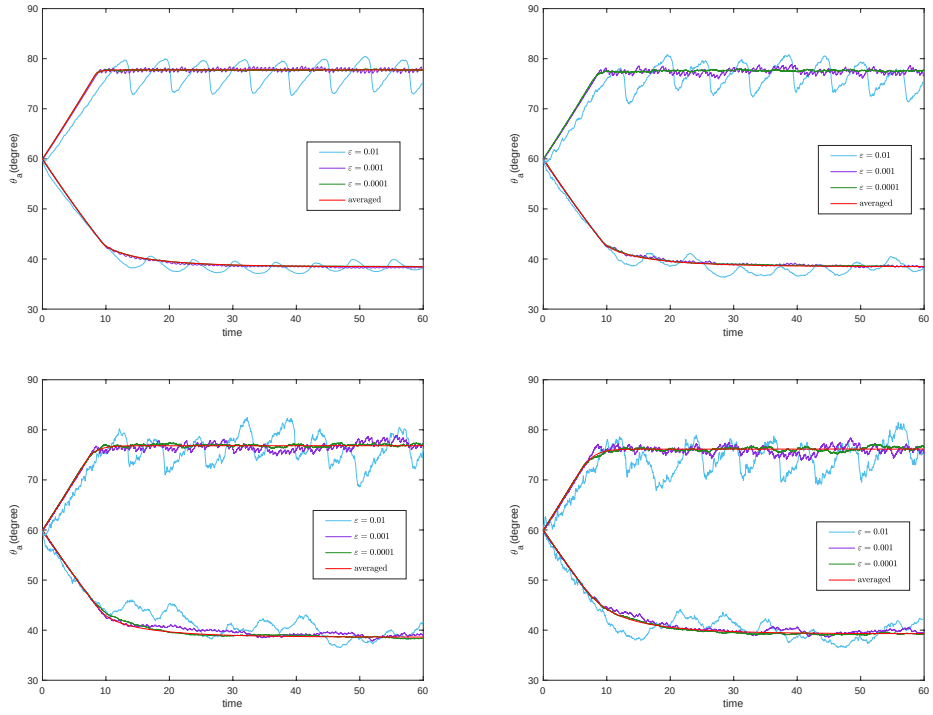

FIG. 7. *Receding and advancing dynamics for* $\varepsilon = 0.05, 0.01, 0.001$ *and* 0.0001 *and the averaged contact angle. Upper left panel:* $\sigma = 0.1$. *Upper right panel:* $\sigma = 0.3$. *Lower left panel:* $\sigma = 0.6$. *Lower right panel:* $\sigma = 0.8$.

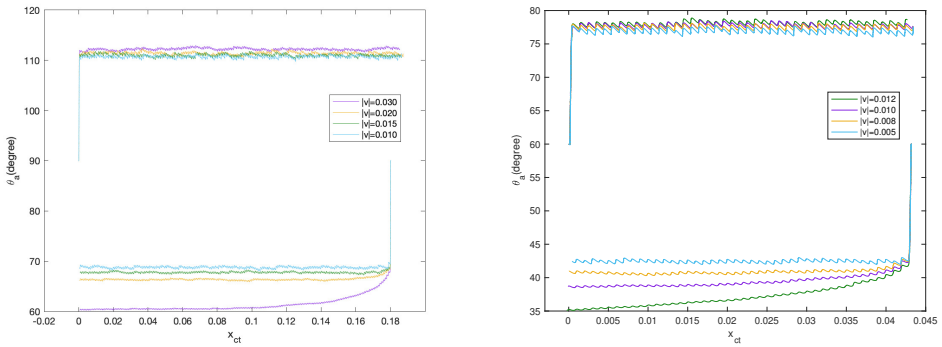

FIG. 8. *Velocity dependence of the CAH phenomena with* $\varepsilon = 0.001$ *and* $\sigma = 0.1$ *in Example 2 and Example 4.*

6. Conclusions. We study the dynamic contact angle hysteresis of wetting on geometrically and chemically rough surfaces. We derive averaged systems for both a deterministic model and a stochastic model. For the deterministic model, we derive an explicit formula (24) for the apparent contact angles in steady states. The equation (24) indicates that the apparent contact angles depends on the contact line velocity as well as the harmonic averaging of the geometrical and chemical inhomo-

geneity near the contact line. It can be used as a dynamic boundary condition for contact angle hysteresis in general cases, coupled with the two-phase Navier-Stokes equation. For the stochastic model, the stochastic thermal forces play an important role and a similar formula (38) is derived. The relations between the stochastic models and the deterministic models are also discussed. We provide rigorous analysis for the multi-scale analysis by proving the convergence of the original systems to the averaged systems when the roughness coefficient goes to zero. Numerical examples are presented to verify the theoretical results.

In this study, we focus mainly on two dimensional problems. The three dimensional problems can be discussed by combining the results in 2D with some previous homogenization results [33]. This is very complicated and will be left for future work.

Appendix A. Derivation of the ODE system for the capillary problem on a moving fiber. We first use the equation (4) for the liquid-air interfaces. On the contact line, we have the consistent condition

$$\begin{aligned} z_{ct} &= h(t) - \tilde{R}(z_{ct},t)\cos\theta_a \ln \frac{\tilde{R}(z_{ct},t) + \sqrt{\tilde{R}(z_{ct},t)^2 - \tilde{R}^2(z_{ct},t)\cos^2\theta_a}}{\tilde{R}(z_{ct},t)\cos\theta_a} \\ &= h(t) - \tilde{R}(z_{ct},t)\cos\theta_a \ln \frac{1+\sin\theta_a}{\cos\theta_a}. \end{aligned}$$

Substitute the equation to (4) and eliminate $h(t)$, we have

$$H(r) = z_{ct} - \tilde{R}(z_{ct},t)\cos\theta_a \ln \frac{r + \sqrt{r^2 - \tilde{R}^2(z_{ct},t)\cos^2\theta_a}}{\tilde{R}(z_{ct},t)(1+\sin\theta_a)}. \tag{46}$$

Far from the fiber, the liquid surface becomes flat. We set $H(r_c) = 0$ for a capillary length r_c. Then we have $H(r_c) = 0$. This leads to an equation

$$z_{ct} - \tilde{R}(z_{ct},t)\cos\theta_a \ln \frac{r_c + \sqrt{r_c^2 - \tilde{R}^2(z_{ct},t)\cos^2\theta_a}}{\tilde{R}(z_{ct},)(1+\sin\theta_a)} = 0. \tag{47}$$

The equation gives a relation between the contact angle and contact point. We will use the equation and the equation (3) to derive a complete system to describe the dynamic contact angle.

Actually, notice that the contact line velocity is given by $v_{ct} = (\dot{z}_{ct} - v_w)/\cos\theta_g$. The equation (3) is reduced to

$$\dot{z}_{ct} - v_w = \frac{\gamma \mathcal{F}(\theta_d)\cos\theta_g}{\mu}(\cos\theta_Y - \cos\theta_d). \tag{48}$$

Then the derivative for the equation (47) gives a relation that

$$\dot{\theta}_a = -g_1(\theta_a, z_{ct}, t)\Big(g_2(\theta_a, z_{ct}, t)(\dot{z} - v_w) + v_w\Big) \tag{49}$$

where

$$\begin{aligned} g_1(\theta_a, z_{ct}, t) &= \frac{1}{\tilde{R}(z_{ct},t)\big(\sin\theta_a \mathcal{G}(\theta_a, z_{ct}, v_w) + 1\big)} \\ g_2(\theta_a, z_{ct}, t) &= 1 - R_1'(\frac{z_{ct} - v_w t}{\varepsilon})\mathcal{G}(\theta_a, z_{ct}, t)\cos\theta_a. \end{aligned}$$

and

$$\mathscr{G}(\theta_a, z_{ct}, t) = \ln \frac{r_c + \sqrt{r_c^2 - \tilde{R}^2(z_{ct}, t)\cos^2\theta_a}}{\tilde{R}(z_{ct}, t)(1+\sin\theta_a)} - 1 \\ - \frac{\tilde{R}^2(z_{ct}, t)\cos^2\theta_a}{(r_c + \sqrt{r_c^2 - \tilde{R}^2(z_{ct}, t)\cos^2\theta_a})\sqrt{r_c^2 - \tilde{R}^2(z_{ct}, t)\cos^2\theta_a}}.$$

If $r_c \gg R_0$, the formula can be further simplified to

$$\mathscr{G}(\theta_a, z_{ct}, t) = \ln \frac{2r_c}{\tilde{R}(z_{ct}, t)(1+\sin\theta_a)} - 1.$$

To further simplify the equations, we can introduce a new variable $\hat{z}_{ct} = z_{ct} - v_w t$, which is actually the vertical coordinate of the contact line in a coordinate system moving with the fiber. Then the equations (48) and (49) are reduced to the equation (5).

Appendix B. Asymptotic Approximations of Stochastic System's Integrals. We show how to calculate the averaged stochastic dynamics (35) numerically. Although we present the exact formula for the invariant measure in Section 4.1, it is difficult to use when σ is very small. In this case we consider the asymptotic approximation of the averaged equation. As discussed in Section 4.2, we have two different cases: in the first case, $A > 0$ or $A < 0$ always holds; and in the second case, there exists at least one y_0 such that $A(\Theta, y_0) = 0$.

Firstly, when A does not have zeros, by using the Watson' lemma, we have the following approximation:

$$\frac{\mathrm{d}\Theta}{\mathrm{d}t} = \int_{\mathbb{T}} B(\Theta, y)\rho^{\infty}(\Theta, y)\mathrm{d}y \\ = C_1 \int_{\mathbb{T}} B(\Theta, y)\Big(\frac{1}{A(\Theta, y)} + \sigma^2 \frac{2A(\Theta, y)f(y)f'(y) - f(y)A'(\Theta, y)}{2A^3(\Theta, y)}\Big)\mathrm{d}y$$

where the constant $C_1 = \Big(\int_{\mathbb{T}} \frac{1}{A(\Theta,y)} + \sigma^2 \frac{2A(\Theta,y)f(y)f'(y) - f(y)A'(\Theta,y)}{2A^3(\Theta,y)}\mathrm{d}y\Big)^{-1}$.

In second case, there are a stable point y_0 of the function A such that $A(\Theta, y_0) = 0$ and $A'(y_0) < 0$. By using Laplace method, we obtain the following approximation:

$$\frac{\mathrm{d}\Theta}{\mathrm{d}t} = \int_{\mathbb{T}} B(\Theta, y)\rho^{\infty}(\Theta, y)\mathrm{d}y \\ = -\sigma \frac{g(\Theta)(1+p(\Theta, y))f^2(y_0)\sqrt{A'(0)}A'(y_0)}{C_2 4\pi A'(y_0)f(0) - 2f(y_0)\sqrt{-A'(0)A'(y_0)}}(\frac{2}{\sqrt{\pi}} + \sqrt{\pi}) - g(\Theta)v$$

where the constant $C_2 = \mathrm{sgn}(V(1) - V(0))\exp(\frac{\min\{V(0), V(1)\}}{\sigma^2})$ and $V(y) = -\int_0^y \frac{2A}{f^2}\mathrm{d}y$.

In the numerical examples in Section 5, we use the asymptotic approximations when the noise coefficient $\sigma = 0.1$ and 0.3. And we calculate the averaged dynamics using the exact formula (36) for the invariant measure when the noise coefficient $\sigma = 0.6$ and 0.8.

REFERENCES

[1] G. Alberti and A. DeSimone. Wetting of rough surfaces: A homogenization approach. Proc. R. Soc. A, 451:79–97, 2005.

[2] G. Alberti and A. DeSimone. Quasistatic evolution of sessile drops and contact angle hysteresis. Arch. Rational Mech. Anal., 202(1):295–348, 2011.

[3] Terence D Blake. The physics of moving wetting lines. Journal of Colloid and Interface Science, 299(1):1–13, 2006.

[4] Daniel Bonn, Jens Eggers, Joseph Indekeu, Jacques Meunier, and Etienne Rolley. Wetting and spreading. Reviews of Modern Physics, 81(2):739, 2009.

[5] L.A. Caffarelli and A Mellet. Capillary drops: contact angle hysteresis and sticking drops. Cal. Var. Partial Differ. Equ., 29(2):141–160, 2007.

[6] X. Chen, X.-P. Wang, and X. Xu. Effective contact angle for rough boundary. Physica D, 242:54–64, 2013.

[7] R. Cox. The dynamics of the spreading of liquids on a solid surface. Part 1. Viscous flow. J. Fluid Mech., 168:169–194, 1986.

[8] P.G. de Gennes, F. Brochard-Wyart, and D. Quere. Capillarity and Wetting Phenomena. Springer Berlin, 2003.

[9] M. Doi. Onsager priciple as a tool for approximation. Chinese Phys. B, 24:020505, 2015.

[10] Jaroslaw W Drelich, Ludmila Boinovich, Emil Chibowski, Claudio Della Volpe, Lucyna Hołysz, Abraham Marmur, and Stefano Siboni. Contact angles: History of over 200 years of open questions. Surface Innovations, 8(1–2):3–27, 2019.

[11] William M Feldman and Inwon C Kim. Liquid drops on a rough surface. Communications on Pure and Applied Mathematics, 71(12):2429–2499, 2018.

[12] Yuan Gao and Jian-Guo Liu. Gradient flow formulation and second order numerical method for motion by mean curvature and contact line dynamics on rough surface. Interfaces and Free Boundaries, 23(1):103–158, 2022.

[13] Yuan Gao and Jian-Guo Liu. Projection method for droplet dynamics on groove-textured surface with merging and splitting. SIAM Journal on Scientific Computing, 44(2):B310–B338, 2022.

[14] R. Golestanian and E. Raphaël. Roughening transition in a moving contact line. Phys. Rev. E, 67(3):031603, 2003.

[15] D. Guan, Y. Wang, E. Charlaix, and P. Tong. Asymmetric and speed-dependent capillary force hysteresis and relaxation of a suddenly stopped moving contact line. Phys. Rev. Lett., 116(6):066102, 2016.

[16] D. Guan, Y. Wang, E. Charlaix, and P. Tong. Simultaneous observation of asymmetric speed-dependent capillary force hysteresis and slow relaxation of a suddenly stopped moving contact line. Phys. Rev. E, 94(4):042802, 2016.

[17] J. F. Joanny and P.-G. De Gennes. A model for contact angle hysteresis. J. Chem. Phys., 81(1):552–562, 1984.

[18] Song Lu and Xianmin Xu. An efficient diffusion generated motion method for wetting dynamics. Journal of Computational Physics, 441:110476, 2021.

[19] A. Mellet and J. Nolen. Capillary drops on a rough surface. Interfaces Free Boundaries, 14(2):167–184, 2012.

[20] Grigoris Pavliotis and Andrew Stuart. Multiscale methods: averaging and homogenization. Springer Science & Business Media, 2008.

[21] T. Qian, X.P. Wang, and P. Sheng. Molecular scale contact line hydrodynamics of immiscible flows. Phys. Rev. E, 68:016306, 2003.

[22] D. Quere. Wetting and roughness. Annu. Rev. Mater. Res., 38:71–99, 2008.

[23] Elie Raphael and Pierre-Gilles de Gennes. Dynamics of wetting with nonideal surfaces. the single defect problem. The Journal of chemical physics, 90(12):7577–7584, 1989.

[24] W. Ren and W. E. Boundary conditions for the moving contact line problem. Phys. Fluids, 19(2):022101, 2007.

[25] W. Ren and W. E. Contact line dynamics on heterogeneous surfaces. Phys. Fluids, 23:072103, 2011.

[26] Y. D. Shikhmurzaev. Capillary flows with forming interfaces. Chapman and Hall/CRC, 2007.

[27] Y. D. Shikhmurzaev. Moving contact lines and dynamic contact angles: a litmus test for mathematical models, accomplishments and new challenges. The European Physical Journal Special Topics, 229(10):1945–1977, 2020.

[28] Anatoliĭ Vladimirovich Skorokhod. Asymptotic methods in the theory of stochastic differential equations, volume 78. American Mathematical Soc, 2009.

[29] J. H. Snoeijer and B. Andreotti. Moving contact lines: scales, regimes, and dynamical transi-

tions. Annual Rev. Fluid Mech., 45:269–292, 2013.
[30] Dong Wang, Xiao-Ping Wang, and Xianmin Xu. An improved threshold dynamics method for wetting dynamics. Journal of Computational Physics, 392:291–310, 2019.
[31] X.P. Wang, T. Qian, and P. Sheng. Moving contact line on chemically patterned surfaces. J. Fluid Mech., 605:59–78, 2008.
[32] Gershon Wolansky. Contact angles of liquid drops subjected to a rough boundary. SIAM Journal on Mathematical Analysis, 51(3):2286–2305, 2019.
[33] X. Xu. Modified wenzel and cassie equations for wetting on rough surfaces. SIAM J. Appl. Math., 76(6):2353–2374, 2016.
[34] X. Xu and X. Wang. Theoretical analysis for dynamic contact angle hysteresis on chemically patterned surfaces. Physics of Fluids, 32:112102, 2020.
[35] X. Xu and X. P. Wang. Analysis of wetting and contact angle hysteresis on chemically patterned surfaces. SIAM J. Appl. Math., 71:1753–1779, 2011.
[36] X. Xu and X.-P. Wang. Theoretical analysis for dynamic contact angle hysteresis on chemically patterned surfaces. Physics of Fluids, 32(11):112102, 2020.
[37] X. Xu, Y. Zhao, and X.-P. Wang. Analysis for contact angle hysteresis on rough surfaces by a phase field model with a relaxed boundary condition. SIAM J. Appl. Math., 79:2551–2568, 2019.
[38] Jiaqi Zhang and Pengtao Yue. A level-set method for moving contact lines with contact angle hysteresis. Journal of Computational Physics, page 109636, 2020.
[39] Zhen Zhang and Xianmin Xu. Effective boundary conditions for dynamic contact angle hysteresis on chemically inhomogeneous surfaces. Journal of Fluid Mechanics, 935, 2022.